



Implementation of an Automated Film Deposition Equipment under the sol/gel Dip-Coating Technique^a

Implementación de un equipo automatizado de deposición pelicular bajo la técnica sol/gel dip-coating

Received: January 22, 2020 | Accepted: June 16, 2021 | Published: July 25, 2022

Laura Andrea Florez-Bedoya *

Universidad Tecnológica de Pereira, Pereira, Colombia

ORCID: <https://orcid.org/0000-0002-9932-398X>

Laura Estefanía Mora-Joaqui

Universidad Tecnológica de Pereira, Pereira, Colombia

ORCID: <https://orcid.org/0000-0001-5110-9899>

Beatriz Cruz-Muñoz

Universidad Tecnológica de Pereira, Pereira, Colombia

ORCID: <https://orcid.org/0000-0002-7023-1942>

Rubén José Dorantes-Rodríguez

Universidad Autónoma Metropolitana - Unidad Azcapotzalco, Ciudad de México, México

ORCID: <https://orcid.org/0000-0001-8636-1306>

Sebastián Ospina-Castro

Universidad Tecnológica de Pereira, Pereira, Colombia

ORCID: <https://orcid.org/0000-0003-2385-7691>

Alexander Ríos-Gaviria

Servicio Nacional de Aprendizaje -SENA, Pereira, Colombia

ORCID: <https://orcid.org/0000-0001-5500-4218>

^a Research paper - Article of scientific and technological investigation

* Corresponding author. E-mail: florezlaura@utp.edu.co

DOI: <https://doi.org/10.11144/javeriana.iued26.iafd>

How to cite this article:

L. A. Florez-Bedoya, L. E. Mora-Joaqui, B. Cruz-Muñoz, R. J. Dorantes-Rodríguez, S. Castro-Ospina, A. Ríos-Gaviria "Implementation of an automated film deposition equipment under the sol/gel dip-coating technique" Ing. Univ. vol. 26, 2022. <https://doi.org/10.11144/javeriana.iued26.iafd>

Abstract

We present the design, construction, and implementation of thin film deposition equipment based on the Sol/Gel dip-coating technique for the fabrication of coatings under controlled deposition conditions and working environment at ambient temperature and pressure. The deposition system includes a 304 stainless steel structure and a moving platform that holds the substrate and is transported along vertical axes at a deposition distance of up to 30 cm in height. The mechanical and electronic design was considered, using computer-aided development and dimensional validation (for the structure and the motion transmission system) and the programming of the system using the Arduino platform. The design focused on the deposition speed control for the functional equipment operations, whose operating principle is based on a PWM scheme, achieving an immersion/extraction speed parameter in ranges between 1.5 cm/s and 3.5 cm/s (with a resolution of ± 0.2 cm/s). The operation of the equipment and the reproducibility of the deposits were tested by studying the optical properties of CuCoMn coatings on glass. A substrate immersion/extraction speed of 1.5 cm/s and precursor agitation time (0.83 h - 0.98 h) were used, obtaining absorbances higher than 90%. In conclusion, the implemented prototype will allow the research group to produce reproducible thin films of better quality than those made manually, which can be produced at a low cost and offer the possibility of sustainable maintenance of the equipment.

Keywords: Dip-coating, open-source programming, PWM, sol-gel, thin films.

Resumen

Se presenta el diseño, construcción e implementación de un equipo de depósito de películas delgadas basado en la técnica Sol/Gel dip-coating destinado a la fabricación de recubrimientos bajo condiciones de depósito controlados y entorno de trabajo a temperatura y presión ambiente. El sistema de depósito incluye una estructura en acero inoxidable 304 y una plataforma de movimiento que sujeta el sustrato y se transporta a lo largo de ejes verticales una distancia de depósito de hasta 30 cm de altura. Se consideró el diseño mecánico y electrónico, empleando un desarrollo asistido por computador y validación dimensional (para la estructura y el sistema de transmisión de movimiento) además de la programación del sistema empleando la plataforma Arduino. Para las operaciones de funcionamiento del equipo, el diseño se enfocó en el control de velocidad de depósito, cuyo principio de operación se basa en un esquema PWM, logrando un parámetro de velocidad de inmersión/extracción, en rangos entre 1.5 cm/s y 3.5 cm/s (con resolución de ± 0.2 cm/s). Se comprobó la operación del equipo y la reproducibilidad de los depósitos mediante el estudio de las propiedades ópticas de recubrimientos de CuCoMn sobre vidrio. Se empleó una velocidad de inmersión/ extracción del sustrato de 1.5 cm/s y tiempo de agitación de los precursores (0.83 h - 0.98 h), obteniendo absorbancias mayores de 90%. En conclusión, el prototipo implementado permitirá al grupo de investigación producir películas delgadas reproducibles y de mejor calidad que las realizadas manualmente, que puedan producirse a bajo coste y que ofrezcan la posibilidad de un mantenimiento sostenible del equipo.

Palabras clave: Dip-coating, películas delgadas, programación de código abierto, PWM, sol-gel.

Introduction

Of the different techniques used to manufacture thin films, such as chemical vapor deposition (CVD), pulsed laser deposition, sputtering, etc., the Sol-Gel chemical route is one of the easiest to apply. This technique stems from a colloidal solution formed from the precursor elements of the compound to be obtained. The substrate is immersed/extracted from the solution at a constant speed during the deposition process and subsequently subjected to heat treatment. These parameters determine the physical and chemical properties of the film. A constant linear velocity influences the thickness of the thin films obtained from the syntheses due to the influence of gravitational forces during the extraction process, which goes beyond the effect caused by the drying or dipping time, as formerly demonstrated [1].

The equipment known as dip coater is designed to operate exclusively for the dipping of a substrate (an element that requires modification) and therefore lends itself to automation since the process is relatively simple and repetitive. The thickness of the coating is determined by the speed of extraction, the viscosity of the liquid is produced by the conditions in which the precursor chemical solutions are prepared, and the environment of the deposit (temperature and ambient humidity) [2]. Pérez Saura [3] and Adámek [4] stated how efficient a dip coater is, mainly caused by the minimal waste production in the equipment, as any excess solution returns to the dipping vessel to be used in the next layer application.

Easy-access and cost-effective instrumentation translate into process automation using programmable development platforms and adaptable electronic components, whose open-source environment allows microcontrollers to be customized to a system's needs. As a result, free hardware, prototypes, or instruments that improve the quality of processes and applications are obtained [5].

Different deposition equipment based on the dip-coating technique have been repeatedly implemented in several ways [3]-[7], showing its reliable and cost-effective implementation. Segura et al. [6] proposed dip coater equipment with a motion system formed by gears of different radii, whereby motor speed is controlled by varying the pulse width according to the PWM technique (Pulse Width Modulation) and the use of Arduino software. Alternatively, another study found that speed control could be formulated using the PID algorithm (Proportional-Integral and Derivative). The difference lies in the rigor with which this procedure verifies the magnitude to be controlled. The deposition process must be monitored and controlled, considering the need to deposit thin films with reproducible properties. In this case, automation was performed at a low cost using open-source microcontrollers [7].

This document presents the design and control strategies used to construct dip coater equipment to address the lack of this type of equipment for the development of materials and applying low-cost instrumentation. Specifically, three objectives were addressed: the first is the development of the mechanical and electronic facets, which range from motion transmission to programming in microcontrollers.

Reference is also made to adjusting the engine speed used for instrumentation depending on the variation of the lifecycle of a generated signal, comparing the theoretical values defined by formulae with the experimental values obtained by measurement in the system. Moreover, equipment behavior is observed by depositing CuCoMn coatings on glass substrates at a fixed speed and by varying the stirring time of the sol-gel synthesis to study its influence on the solar radiation absorption response in the UV-Vis range. Solar absorbers (with a high absorption coefficient, greater than 90%) primarily convert solar energy into heat. This heat reduces the electricity used for heat production and can save energy or serve as a possible replacement for natural gas (fossil fuel). Commonly, copper pipes are used for heat transfer by liquids. Thus, ideally, manufacturing coatings (that improve the solar absorption of metallic surfaces) would imply an increase in the efficiency of absorption and use of solar radiation [8]. The following sections discuss the entire design and development process and an initial test of the equipment operation with coatings deposited in triplicate to determine optical reproducibility.

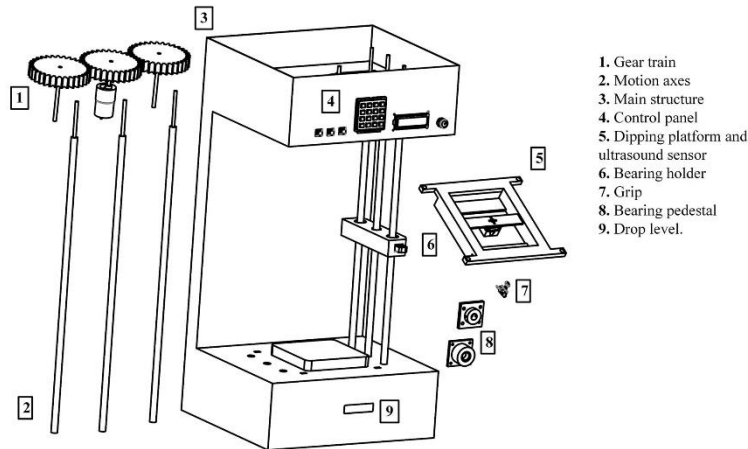
Materials and methods

Dip-coater construction: Design of structure and mechanical components

Two approaches were considered in the design of the dip coater equipment: the mechanical system in charge of motion and the electronic system, whose function is to implement a programming algorithm for speed control. The mechanical design is the product of prototyping and iterations, which can validate the movement and the form and use, based on a CAD design in SolidWorks 2016.

The fundamental purpose of the structure is to support the different mechanisms that underlie the motion transmission system. As a result, a 3D render is presented where the CAD model of the structural system and its different components are displayed in an exploded view, as shown in Figure 1.

Figure 1. Exploded 3D structure rendering



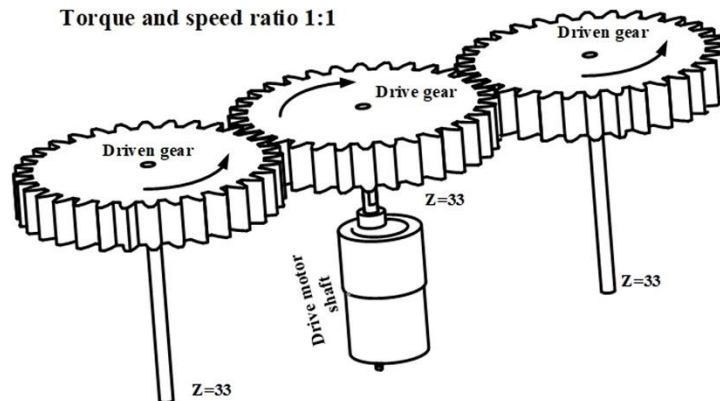
Source: Own source

The construction of the first prototype was based on a 3D printing system (or CNC), and the spindle or threaded shaft provides the motion power-driven by the direct current motor. The mechanical components were mostly printed in 3D on ABS (Acrylonitrile Butadiene Styrene) and PLA (Polylactic Acid), as this type of implementation minimizes assembly, type of manufacture, and areas of weakness. It maximizes the performance of the mechanical systems by optimizing the structure of the components found in the integrated system.

Motion system

A simple gear train was designed (see Figure 2), consisting of a central shaft coupled to the DC motor, which transmits motion to the system. In addition to the mechanical system, there are two driven gears, which transmit power to the spindles that allow the vertical motion of the dipping platform.

Figure 2. Simple gear train.



Source: Own source

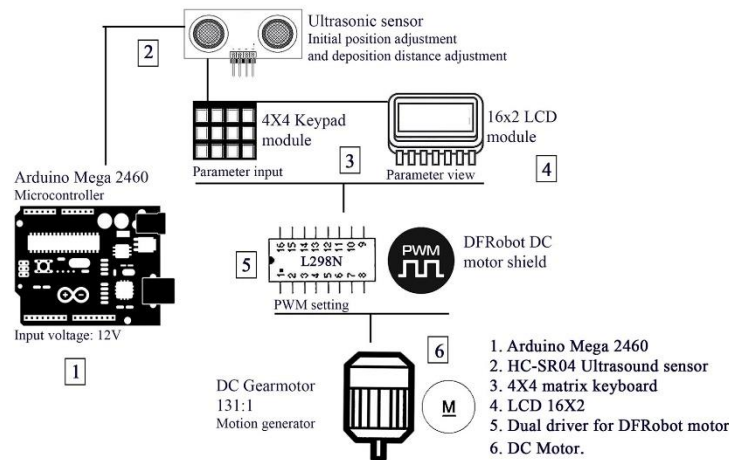
The motion transmission system was calculated the required transmission ratio [9]. The transmission ratio involves the diameter of the gears and the circular speed of each of them. According to the structure of the support, it was decided that the transmission ratio would be unitary, where the diameters of the gears are equal and measure 62 mm. The driver unit comprises three axes: a driving shaft and two driving axes, with a distance between their centers of 67 mm. Based on this information, the gears and their location within the system were designed in CAD software, as shown in Figure 2.

Electric circuit and component design

The development of the electronic components consists of the modeling of a systematized process based on open-source software. In itself, the algorithm contains the operational electronic structure of the system, using C++ language features and commands, where electronic components such as actuators, controllers, and peripherals are adjusted to obtain a configurable device or a rapid prototype of digital microcontrollers [10].

This approach offers significant advantages, such as a simple programming environment adaptable to any operating system allowing code manipulation for maintenance or improvement of the operating algorithm. It also served as an integrable platform that allows using different hardware devices and sensors designed exclusively to be coupled to this type of electronic card. In order to implement this idea, a complete integrated circuit design must be derived from the available software and hardware (Eagle, Arduino, CCS Compiler) (see Figure 3).

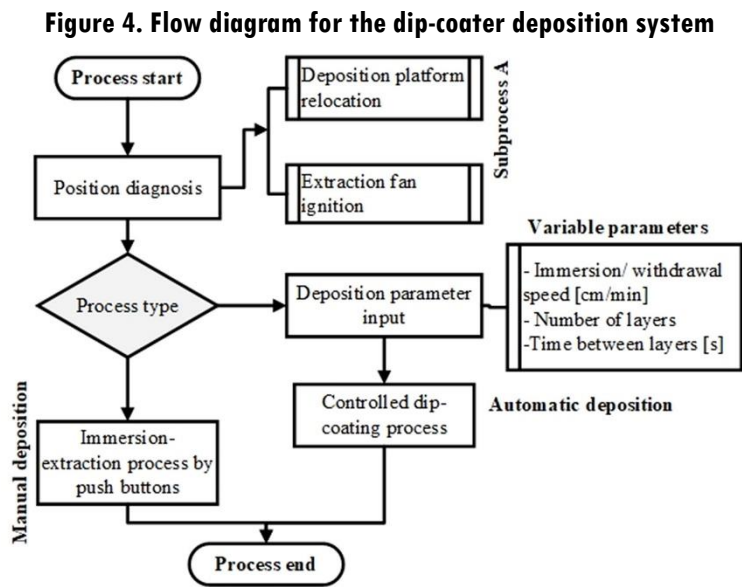
Figure 3. Electronic operating diagram for the deposit system



Source: Own source

The following process was carried out: function design, iterative verification, and debugging of the implemented electronic system to develop the electronic system of the dip coater automated equipment.

The flow diagram shown in Figure 4 illustrates the operation process of a film coating system. This procedure is established from the literature on similar systems [11]. The development of the algorithm using free software platforms such as Arduino and the use of pre-assembled hardware allows tests to be carried out on the proposed code, where the working capacity of the equipment's microcontrollers was determined.



Source: Own source

Statistical analysis of the speed variable

An accuracy specification for a measurement represents the degree of uncertainty caused by systematic errors of a particular measuring instrument. For the determination of the experimental error of the equipment speed, the correlated input and output magnitudes are expressed and then subjected to statistical analysis to calculate the expanded uncertainty of the system at a confidence level or coverage probability of 95% (where the general formula can be expressed as, $U_e=U_c*k$) [12]. Finally, the corresponding degree of uncertainty will be associated with each speed value for the operating speed parameters.

For the accuracy test, four rotational speed measurements for each gear of the movement system were taken, and the speed was varied with the change of pulses in the duty cycle for the DC motor. A Mastech DT2234C tachometer with a resolution of 0.1 rpm was used to perform the rotational speed measurement. The radius of each gear was measured with a Mitutoyo, model CD-S6 "CP, series 1964, with a resolution of 0.001 cm.

CuCoMn synthesis by sol-gel

Following the procedure formerly reported in the literature [13], a citric acid-supported sol-gel variation was used to form absorbing surfaces on certain substrates. The reagents cobalt nitrate [$\text{Co}(\text{NO}_3)_2 \cdot 6\text{H}_2\text{O}$, Merck, 99.0%], manganese nitrate [$\text{Mn}(\text{NO}_3)_2 \cdot 4\text{H}_2\text{O}$, Merck, 98.5%] and copper chloride [$\text{CuCl}_2 \cdot 2\text{H}_2\text{O}$, Merck, 99.0%] were dissolved in absolute ethanol [$\text{C}_2\text{H}_5\text{OH}$, Merck, 99.9%] in relation to Co:Cu:Mn = 1:3:3. To enable hybrids obtaining citric acid (AC) was added following the ratio $\text{AC}/\text{M}+(\text{metal ions})= 1.2$. The solution was mixed in a magnetic stirrer at a constant temperature for 1 h. To improve solvent interaction with metal ions and achieve the formation of strong metal complexes [14], ethylene glycol (EG) [$\text{C}_2\text{H}_6\text{O}_2$, Carlo Erba, 99%] is added to the molar ratio $\text{EG}/\text{AC}= 0.8$, and 1 wt% Hydroxyethyl cellulose -HEC [Merck, 92.0%].

The CuCoMn resulting solution was deposited at 1.5 cm/s (as the minimum speed value provided by the equipment) at different stirring times (Table 1). Glass slides (75 mm X 25 mm) were used as substrates, which were previously prepared by cleaning using industrial soap, deionized water (18.2 M Ω), and an ultrasonic bath in acetone and methanol for 20 min. CuCoMn coatings were thermally treated in a tubular muffle in the presence of Ar for 30 min at 450 °C (the temperature chosen was based on the DTG/TGA curves to ensure the stable phases of each reagent while avoiding the melting point of the glass). Thermogravimetric analysis (thermal decomposition and annealing temperature) and derived thermogravimetry were performed using a simultaneous DSC-TGA thermal analyzer (TA instruments SDT 650). For each sample obtained, reflectance and transmittance spectra were measured using a Thermo Scientific - Evolution 220 UV-VIS spectrophotometer with an integration sphere (both types of spectra were used to find the indirect absorbance for all samples [15]).

Lastly, the surface images of the films were recorded using an IX53 Olympus inverted binocular microscope, while the thickness was obtained from a CEM DT-156 thickness meter. In order to observe the reproducibility behavior of the constructed dip coating equipment built for this experiment, three deposits were made, and the spectra were taken at a point located at the same distance from the upper edge of each substrate.

Results and discussion

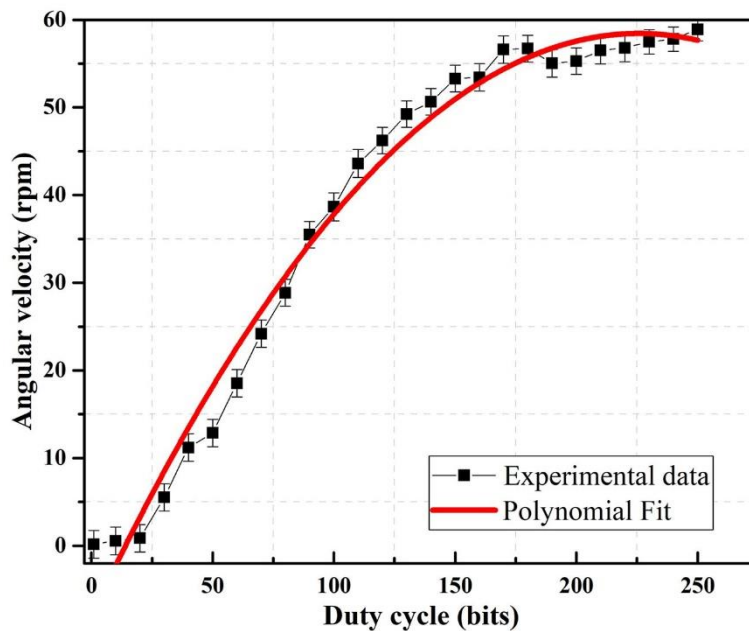
Speed control via PWM

The DC motor is generally the most commonly used type of direct current motor because the rotational speed it produces is easy to control. It consists of a stationary body called a "stator," and a constantly moving body called a "rotor" [16]. The rotational speed depends on the

interaction between the magnetic fields generated by both bodies. By controlling the current flow through the windings, the magnetic flux can be controlled, thus controlling the motor speed.

PWM technique, as mentioned earlier [17], [18]; is implemented to design the automated control system for the dip coater prototype, which helps reduce the likelihood of failure by providing a constant speed that controls the magnetic flux provided to the engine. This method is in charge of emulating a type of analog signal (by pulses), varying the cycle of work related to the time inactive state of the same signal [19]. Controlling is performed on the actuator, connected to an H bridge driver that modifies the pulses on the mainboard (Arduino Mega 2560). Characterization of the motor using indirect measurements in terms of bits (0 -255) and rotational speed (using a digital tachometer on the gear train) made it possible to establish the correlation between the two variables. Based on the tests performed with the tachometer, the angular speed trend was analyzed concerning the pulses' modification in order to establish the speed variation for the deposition system (see Figure 5).

Figure 5. Trend curve of the variation between pulses and angular speed



Source: Own source

The mathematical relationship between these two variables is a second-order equation, as in Equation (1), which is included in the open-source software and describes the equipment's operational algorithm.

$$VRPM = 0.5124b^2 - 0.0013b - 3.593 \quad (1)$$

The function obtained corresponds to the motor's angular speed adjustment. This equation allowed us to choose the necessary ranges to deposit thin films. As shortcuts to the lowest speed rates to deposit (between 1-5 cm/s), the Arduino microcontroller stored these rpm values in specific control panel positions (keypad). Equation (2) calculates linear speed, where r is the radius, and rpm is the angular speed:

$$v = r \times RPM \times 0.105 \quad (2)$$

Error uncertainty for the speed operation parameter

During the uncertainty calculation, two sources of uncertainty in the system variables were taken into account: the random variations of the measurements and the resolution of the measuring instruments. The combined uncertainty U_c of the output variable (linear speed), can be expressed via the standard uncertainties of the input quantities (rotational speed and radius) as follows in Equation (3).

$$U_c = \sqrt{[(0.105 r)^2 * u(rpm)^2] + [(0.105 rpm)^2 * u(r)^2]} \quad (3)$$

Where r is radius, and rpm is the measured rotational speed (uncertainty components). Table 1 shows the result of the determination of the expanded uncertainty U , from the combined uncertainty U_c , with a coverage factor of 1.96 (i.e., 95% of the coverage probability). It can be inferred that the uncertainty of the velocity parameter is ± 0.20 cm/s and that this value remains constant for the speed range of the equipment.

Table 1. Estimation of the expanded uncertainty with coverage factor (k=1.96)

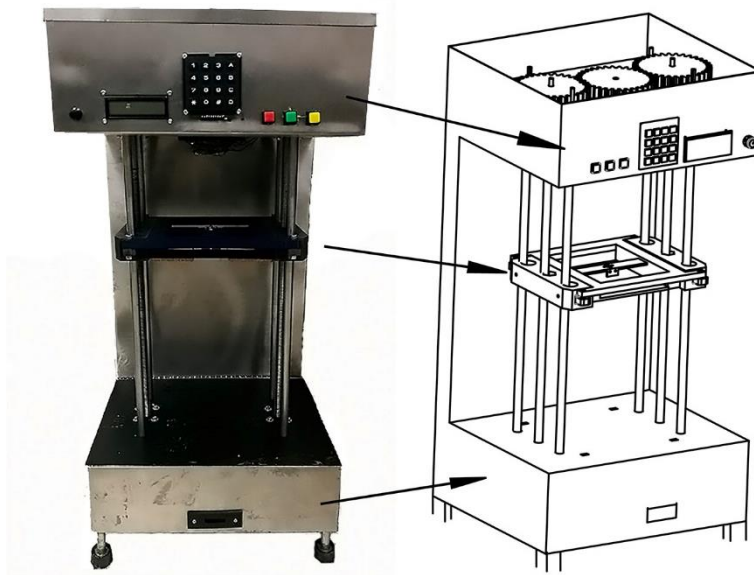
| Theoretical speed [cm/s] | Experimental speed [cm/s] | U_c [cm/s] | k | U_k [cm/s] |
|-----------------------------|------------------------------|-----------------|------|-----------------|
| 1.5 | 1.52 | 0.104 | 1.96 | ± 0.20 |
| 2.0 | 2.04 | 0.106 | 1.96 | ± 0.20 |
| 2.5 | 2.56 | 0.108 | 1.96 | ± 0.20 |
| 3.0 | 3,08 | 0,109 | 1.96 | ± 0.21 |
| 3.5 | 3.60 | 0.109 | 1.96 | ± 0.21 |

Source: Own source

Implementation of dip-coating system (mechanical-electronic articulation)

The main part of the dip-coating structure consists of a 304 stainless steel vertical support with cylindrical linear guide rods and half-inch spindles. Both types of rods are made of commercial steel, and a modified platform printed in 3D (PLA - Polylactic acid material) connected to a sample holder moves along them. The mechanical part itself consists of a gear train in a unit ratio (1:1) of force and speed, where the rotation movement through the guide rods allows the conversion of linear displacement of the sample to the precursor solution. The DC motor powers the driving gear, which transmits the movement from its periphery to the guide rods through pinions or gears of equal dimensions. The prototype built (see Fig. 6) measures (70.3 cm x 35.0 cm x 33.0 cm). Each mechanical component, such as bearing carriers, bearings, etc., was designed using computer-assisted 3D design programs such as SolidWorks 2016, AutoCAD, and Corel Draw, and then printed on ABS (Acrylonitrile Butadiene Styrene), PLA and adapted to the equipment.

Figure 6. Assembled Dip Coater Deposition Equipment



Source: Own source

The function code controls the physical and logical behavior of the dip coating system through a standardized structure based on open loops to regulate both the speed of rotation and the deposition procedure, while the control system's primary function is to maintain a constant speed. The platform's vertical position is detected by an ultrasound sensor HC-SR04 with a measurement resolution of ± 3 mm, for each sound pulse emitted [20]. These signals are recorded in the micro controller's memory for future instructions by the algorithm. The motor speed is controlled by modifying the voltage given to the motor according to the PWM method, and here the analogWrite command of the Arduino microcontroller [21] was used

to drive the motor at different speeds through the generation of pulses in the duty cycle represented on a scale of 0 - 255 bits [22].

The connection between the Arduino and the DC motor is achieved through an Arduino Motor Shield DFRobot, which uses an H L298P bridge that allows motors between 7-12 V to be driven with a maximum current of 2 A. With the coupling of the LM2596 converter module, the regulated voltage necessary for the circuit is guaranteed, from a power supply source with adaptable voltage, both for the Arduino microcontroller and for the DC motor.

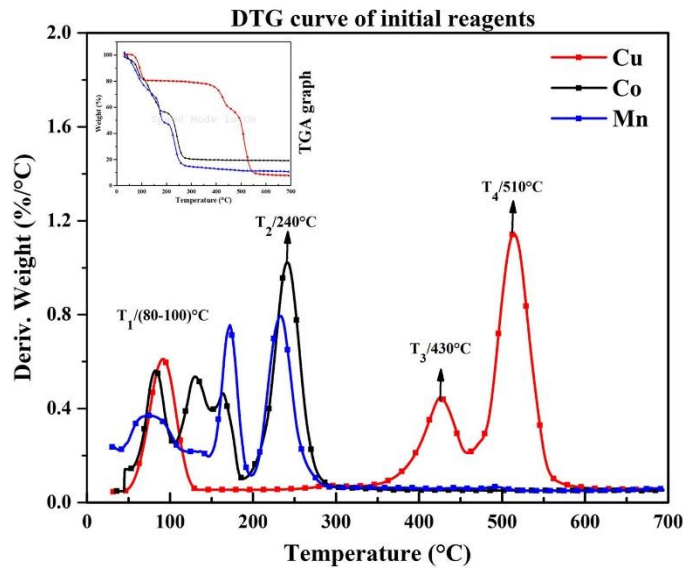
The microcontroller operates the device according to a user's selection, where the linear velocity ranges from 1.5 cm/s to 3.5 cm/s. The velocity parameter error was calculated using indirect measurement uncertainties [23]. Each chosen pulse's rotational velocity was measured under a fixed distance supported by a tachometer, a Vernier calibrator and the Arduino card obtaining a maximum error of ± 0.20 cm/s.

CuCoMn synthesis on glass substrates by dip-coating sol-gel technique

Analysis of thermal decomposition on metallic reagents (TGA/DTG)

The precursor substances were placed in a 90ul (reference for liter capacity in μL) alumina tray and heated to 700 °C at 10 °C/min rate in nitrogen. The thermogravimetric curve (see Fig. 7) for manganese nitrate and cobalt nitrate shows a two-stage decomposition (observable on the DTG curve). The first step starts from 40 °C with peaks between 80 and 100 °C, as a result of an initial dehydration process of the reagents ($[\text{Co}(\text{NO}_3)_2]$ and $[\text{Mn}(\text{NO}_3)_2]$). The complexity of the peaks observed up to 172.28 °C may indicate the formation of hydrates caused by the interaction between the cations of each metallic atom with the water molecules present, permitting a hydrolysis process [24]. At approximately 240 °C, both cobalt nitrate and manganese nitrate decompose completely.

Figure 7. TGA (embedded curve graph) / DTG (continuous line) of initial reagents: Copper chloride, Cobalt nitrate and Manganese nitrate



Source: Own source

In the case of copper chloride, there is a multi-stage decomposition whose intermediates are relatively stable compared to the nitrates used. Initially, the thermogravimetric curve shows a decrease in mass at approximately 93.81 °C, caused by a dehydration process. From this curve, it is also possible to detail the decomposition of copper chloride in two other stages, a peak in the compound's degradation appears at 430 °C, and finally, a main peak of degradation appears in the DTG graph at around 510 °C where decomposition is completed [25].

Optical coatings characterization

The optical properties of the thin film coatings are evaluated based on absorbance (α), obtained indirectly from reflectance and transmittance spectra. Reflectance is the percentage of radiation reflected by a surface. In contrast, the transmittance is a mass/volume phenomenon represented by the measurement of the transmitted light flux through the coating, at the same time normalized by the amount of incident light flux. Any unreflected or transmitted flux is absorbed and is expressed by Equation (4) (where ρ is the reflectance, τ is the transmittance, and α is the absorbance) [26]. Table 1 illustrates the deposit parameters through the dip-coating method.

Table 2. Experimental conditions of CuCoMn synthesis and deposition, where AC: citric acid, M+: metallic ions and EG: ethylene glycol

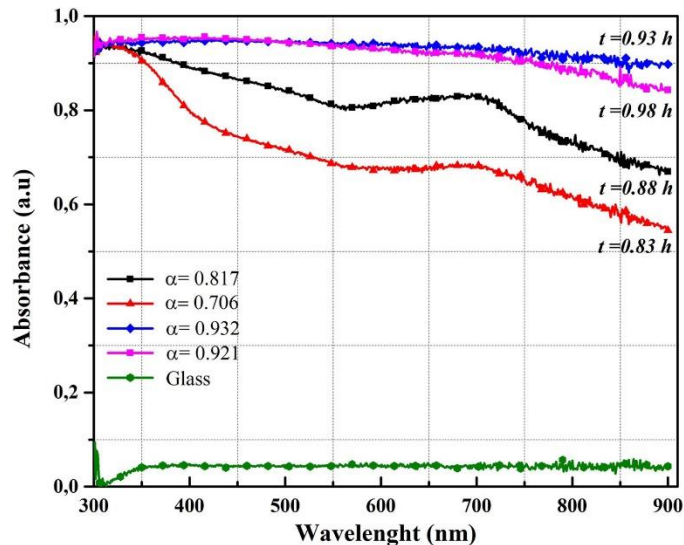
| List of elements in synthesis | | | | | |
|-------------------------------|----------|-------|-------|-------------------|----------------------|
| Sample | Cu:Co:Mn | AC/M+ | EG/AC | Stirring time [h] | Dipping speed [cm/s] |
| 40 017B | 1:3:3 | 1.2 | 0.8 | 0.83 | 1.5 |
| 40 018B | 1:3:3 | 1.2 | 0.8 | 0.88 | 1.5 |
| 40 019B | 1:3:3 | 1.2 | 0.8 | 0.93 | 1.5 |
| 40 020B | 1:3:3 | 1.2 | 0.8 | 0.98 | 1.5 |

Source: Own source

$$\rho + \tau + \alpha = 1 \tag{4}$$

Absorbance spectra for all thin-film coatings on glass substrates within a wavelength range of 300-900 nm are shown in Figure 8. The prepared coatings show high absorbance in the UV-Vis range. However, the CuCoMn deposits at 0.98 h and 0.93 h of agitation present the best optical behavior (in general, 0.921 and 0.932, respectively), considering the carbonization caused by the thermal treatment turning each substrate into opaque surfaces. These resulting coatings could be employed as possible solar absorbers, for example, in low-temperature solar collectors [13].

Figure 8. Absorbance spectra vs. wavelength curve for each sample in Table 1 (deposited with immersion velocity 1.5 cm/s)



Source: Own source

To explain the difference between the optical behavior of the coatings, we carried out other types of characterizations, such as structural or morphological, which are contemplated but

are not the objective of the present article. Using ASTM E308 - 18 [15], the absorbance of each sample was calculated for each area of the solar radiation spectrum (UV, visible light, solar). Table 3 quantitatively and comparatively evaluates the optical behavior of each of the samples.

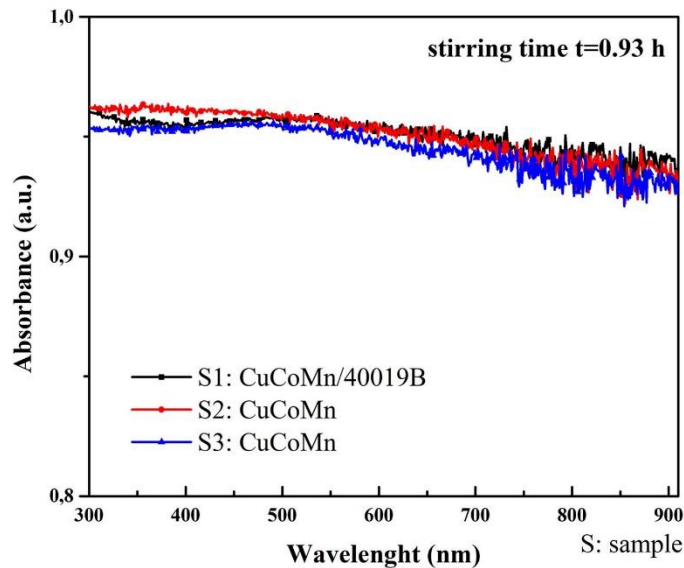
Table 3. Calculation α based on ASTM E308-18 [15]

| Sample: | Absorbance α | | |
|---------|---------------------------|------------------------------|--------------------------------------|
| | Solar global radiation UV | Solar global radiation Solar | Illuminant A 1931 ASTM E308 (90) VIS |
| 40 017B | 94.1 | 81.7 | 92.7 |
| 40 018B | 95.6 | 84.1 | 95.6 |
| 40 019B | 95.7 | 84.1 | 95.7 |
| 40 020B | 95.8 | 84.2 | 95.7 |

Source: Own source

In addition, Figure 9 displays the absorbance spectra for the triplicated samples deposited onto glass (under the same experimental conditions). From the spectra shown, it can be observed that the deposition process proved to be reproducible, irrespective of the samples being processed in different deposition sessions.

Figure 9. Absorbance spectra vs. wavelength curve for three CuCoMn samples (reproducibility test)



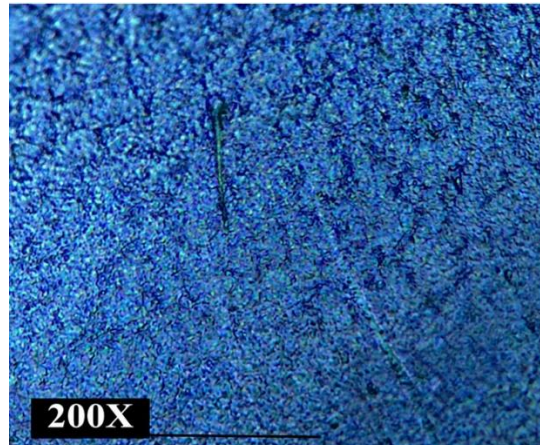
Source: Own source

Thickness and morphology of CuCoMn coatings

One of the samples from the batch of deposited coatings (fabricated under the same experimental conditions for reproducibility) was used to obtain a typical optical microscopic

image (Figure 10). The CuCoMn film synthesized on glass shows small ripple-like patterns along the surface (visible at 200x magnification). In terms of application, the porosity and roughness of the surface can positively influence the heat transfer of a liquid through the solar collector (making metal alloy coatings a potential candidate for these renewable energy applications) [8].

Figure 10. Optical microscopic image of CuCoMn coating (S1:CuCoMn) at 200X



Source: Own source

An in-depth interpretation of the formation of coatings using the dip-coating technique should be extended in another paper, using all the necessary characterization techniques for these materials. Lastly, Table 4 describes the thicknesses measured for the three CuCoMn samples. The average thickness for the three samples was around 0.176 μm .

Table 4. Thickness measurement using CEM DT-156

| Samples | Thickness [μm] |
|-------------------|--------------------------------|
| S1: CuCoMn/40019B | 0.176 |
| S2: CuCoMn | 0.177 |
| S3: CuCoMn | 0.176 |

Source: Own source

Conclusions

Deposition equipment consists of a DC motor that immerses and extracts any sample in the precursor solution. The function code and motor speed control are based on the C++ language for the Arduino microcontroller. Elements such as switches, knobs, keyboard, and LCD screen are attached to the circuit, offering the choice of manual operating parameters such as

linear speed and the number of layers. The equipment is powered by a 21 V charger adapted to deliver the voltage to the Arduino and the DC motor separately. The system allows substrates of any material to be deposited on chemical precursors at linear speeds of between 1.5 cm/s and 3.5 cm/s with an error of ± 0.20 cm/s.

The prototype implemented will allow the research group to produce thin films that are reproducible and have better quality than those made manually, that can be produced at low cost, and that provide the possibility for sustainable equipment maintenance.

It was found that good optical behavior is obtained by depositing CuCoMn coatings on glass substrates (e.g., so that it can be used as an absorbing coating). As for the chemical reaction and carbonization of the thin films resulting from the heat treatment, a hydrolysis process has likely been generated. The presence of alcohol, water, and the esterifying agent (ethylene glycol) would react with the carbon atoms present, adding a carbon layer on each thin film, thus increasing the absorption capacity of the thin films (important property of obtaining solar absorbers).

Finally, the absorption spectra obtained (from a batch of samples deposited under the same conditions) make it possible to determine the reproducibility of the equipment's deposit conditions; and using a thickness gauge, an average thickness of approximately 0.176 μm (176 nm) was obtained for all the samples in this study.

Acknowledgements

The authors are grateful for the financial support from MinCiencias through contests 738 of 2015 and 812 of 2018 for young researchers and innovators. To the Universidad Tecnológica de Pereira (UTP) for the partial funding of this work through the project identified with code 3-18-5 and to its Vice-Rector of Research, Innovation, and Extension for paying the translation of the article.

References

- [1] N. Mahallawy, M. Shoeib and S. Eletriby, "Effect of Sol-Gel Process Parameters on Optical Properties of CuCoMnO_x Selective Coat for Solar Energy Applications," *J. Am. Sci.*, vol. 12, no. 4, pp. 41-48, 2016. <https://doi.org/10.7537/marsjas12041605>
- [2] A. Jilani, M. Abdel-wahab and A. Hammad, "Advance Deposition Techniques for Thin Film and Coating," in *Modern Technologies for Creating the Thin-film Systems and Coatings*, 1st ed. InTech, 2017, pp. 145-152. <https://doi.org/10.5772/65702>
- [3] D. Pérez Saura, "Diseño, construcción y control de una plataforma de experimentación para la automatización de ensayos con muestras de films de polietileno," M.S. thesis, Dept. Ing.

- Sist. Aut., U. Politécnica de Cartagena, España, 2017. [Online]. Available: <http://hdl.handle.net/10317/5597>
- [4] P. Adámek, “Construction of Dip-Coater,” *Edukacja – Technika – Informatyka*, vol. 16, no. 2, pp. 152-156, 2016. <https://doi.org/10.15584/eti.2016.2.20>
- [5] S. Oberloier and J. Pearce, “General Design Procedure for Free and Open-Source Hardware for Scientific Equipment,” *Designs*, vol. 2, no. 1, p. 2, 2017. <https://doi.org/10.3390/designs2010002>
- [6] L. Segura, V. Guerrero, D. Loza Matovelle, and D. Reza, Eds., “Mechanical and Electronic Systems of an Open Source Based Spin and Dip Coater,” in *Rev. Nal. Politécnica*, vol. 37, no. 2, p. 53, 2015. [Online]. Available: https://revistapolitecnica.epn.edu.ec/ojs2/index.php/revista_politecnica2/article/view/561
- [7] I. Medina, A. Loera, L. Arámbula and F. Rizo, “Diseño y fabricación de un aparato para el depósito de películas delgadas por el método de rotación”, in *Investigación y Ciencia*, no. 45, pp. 44-49, 2009. [Online]. Available: <https://www.uaa.mx/investigacion/revista/archivo/revista45/Articulo%207.pdf>
- [8] Y. Zhu, J. Shi, Q. Huang, Y. Fang, L. Wang and G. Xu, “A superhydrophobic solar selective absorber used in a flat plate solar collector,” *RSC Advances*, vol. 7, no. 54, pp. 34125-34130, 2017. <https://doi.org/10.1039/c7ra04238h>
- [9] R. Budynas, J. Nisbett, J. Murrieta Murrieta, E. Alatorre Miguel and J. Shigley, “Engranajes: descripción general,” in *Diseño en ingeniería mecánica de Shigley*, 8th ed. México, D.F.: McGraw-Gill Interamericana, 2008, ch. 13, pp. 667-685.
- [10] M. Cirstea, “Modeling and design of digital electronic systems,” in *Int. Conf. Develop. and Appl. Syst. (DAS)*, 2016. <https://doi.org/10.1109/DAAS.2016.7492596>
- [11] A. Velásquez, J. Urquijo and Y. Gutiérrez, “Diseño y construcción de un reactor mecatrónico para el crecimiento de películas delgadas por la técnica de recubrimiento por inmersión,” *Ing. y Ci.*, vol. 10, no. 20, pp. 93-113, 2014. <https://doi.org/10.17230/ingciencia.10.20.7>
- [12] Bureau International des poids et Measure (BIPM) JCGM 100:2012 Evaluation of measurement data - Guide to the expression of uncertainty in measurement.
- [13] M. He and R. Chen, “Structural and optical properties of CuMnCoOx spinel thin films prepared by a citric acid-based sol-gel dip coating route for solar absorber applications,” *J. Sol-Gel Sci. Technol.*, vol. 74, no. 2, pp. 528-536, 2015. <https://doi.org/10.1007/s10971-015-3630-7>
- [14] A. Bartyzel, “Synthesis, thermal study and some properties of N2O4—donor Schiff base and its Mn(III), Co(II), Ni(II), Cu(II) and Zn(II) complexes,” *J. Therm. Anal. Calorim.*, vol. 127, no. 3, pp. 2133-2147, 2016. <https://doi.org/10.1007/s10973-016-5804-0>
- [15] Standard Practice for Computing the Colors of Objects by Using the CIE System, ASTM E308 - 18, American Society for Testing and Materials, June 2018. [Online]. Available: <https://www.astm.org/Standards/E308.htm>
- [16] A. Faroqi, M. Ramdhani, F. Frasetyio and A. Fadhil, “DC Motor Speed Controller Design using Pulse Width Modulation,” *IOP Conf. Ser.: Mat. Sci. and Eng.*, vol. 434, pp. 1-10, 2018. <https://doi.org/10.1088/1757-899x/434/1/012205>

- [17] J. Sun and Q. Sun, "Design and simulation of PWM DC motor speed regulator based on Proteus," *2015 Int. Conf. Fluid Power and Mechatronics (FPM)*, 2015. <https://doi.org/10.1109/fpm.2015.7337304>
- [18] L. Petru and G. Mazen, "PWM Control of a DC Motor Used to Drive a Conveyor Belt," *Procedia Eng.*, vol. 100, pp. 299-304, 2015. <https://doi.org/10.1016/j.proeng.2015.01.371>
- [19] T. Ng, *Real time control engineering: Systems and Automation*, 1st ed. Singapore: Springer, 2016, pp. 30-45.
- [20] M. Kaur and J. Pal, "Distance Measurement of Object by Ultrasonic Sensor HC-SR04," *IJSRD (International Journal of Scientific Research and Development)*, vol. 3, no. 5, Aug. 2015, Art. no. IJSRDV3I50440. <https://doi.org/10.29130/dubited.634256>
- [21] "Arduino Reference - Function analogWrite", Arduino, 2016. [Online]. Available: <https://www.arduino.cc/reference/en/language/functions/analog-io/analogwrite/>. [Accessed: 14- Oct- 2019].
- [22] I. Agung, S. Huda and I. Wijaya, "Speed control for DC motor with pulse width modulation (PWM) method using infrared remote control based on ATmega16 microcontroller," in *Int. Conf. on Smart Green Technology in Electrical and Information Systems (ICSGTEIS)*, 2014. <https://doi.org/10.1109/icsgteis.2014.7038740>
- [23] P. Dunn, "Uncertainty analysis", in *Measurement and data analysis for engineering and science*, 3rd ed. Boca Raton, Florida: CRC Press, 2014, ch. 7, pp. 229-255.
- [24] B. Małecka, A. Łącz, E. Drożdż and A. Małecki, "Thermal decomposition of d-metal nitrates supported on alumina," *J. Therm. Anal. Calorim.*, vol. 119, no. 2, pp. 1053-1061, 2014. <https://doi.org/10.1007/s10973-014-4262-9>
- [25] M. Nowicki, P. Švec, D. Jackiewicz and R. Szewczyk, "Magnetic Thermogravimetric Analysis of CuCo and CuFe Amorphous Alloys," *Adv. Intel. Syst. Comput.*, pp. 197-204, 2015. https://doi.org/10.1007/978-3-319-15835-8_22
- [26] M. Joly et al., "Optical and structural analysis of sol-gel derived Cu-Co-Mn-Si oxides for black selective solar nanocomposite multilayered coatings," *Sol. Energy Mater. Sol. Cells*, vol. 143, pp. 573-580, 2015. <https://doi.org/10.1016/j.solmat.2015.06.058>